Synthesis and characterization of a liquid-like polythiophene and its potential applications

Yao Lu, Shan Wang, Chuanxi Xiong, Guo-Hua Hu

Version of Record: https://www.sciencedirect.com/science/article/pii/S0379677920308559
Manuscript_9321eb76415ae89e1b4b50d74cab8e5a

Synthesis and Characterization of a Liquid-like Polythiophene and its potential applications

Yao Lu[a], Shan Wang[a]*, Chuanxi Xiong[a]* and Guo-Hua Hu[b]*

[a] State Key Laboratory of Advanced Technology for Materials Synthesis and Processing, and School of Materials Science and Engineering, Wuhan University of Technology, 430070, Wuhan, China.

[b]Université de Lorraine - CNRS, Laboratory of Reactions and Process Engineering (LRGP, UMR 7274), 1 rue Grandville, BP 20451, 54001 Nancy, France.

E-mail: shanwang@whut.edu.cn; cxiong@whut.edu.cn; guo-hua.hu@univ-lorraine.fr.

ABSTRACT: This work presents a method for the synthesis of a liquid-like polythiophene (L-Pth) by chemical oxidative polymerization of thiophene in dichloromethane. $FeCl_3$ was used as an initiator and nonylphenol polyoxyethylene ether (NPES) as a dopant. The structures and physicochemical properties of the L-Pth were characterized by Fourier transform infrared spectroscopy (FTIR), X-ray diffraction (XRD), thermogravimetric analysis (TGA), fluorescence spectroscopy and ultraviolet-visible photometer (UV-vis). Unlike conventional polythiophene, L-Pth is composed of NPES and polythiophene, and part of NPES is doped on the thiophene backbone. It exhibits a liquid-like behavior at room temperature. It is typical of a semiconductor with a relatively high electric conductivity of 1.2 S m^{-1}. Moreover, it turns high-energy blue light (in the ranges of 400 nm to 480 nm) into relative low-energy green light (peak at 515 nm), which makes it a potential filler for preparing a blue light protection film for eyes protection. The combination of the liquid behavior, excellent solubility and good electric conductivity also makes it a promising precursor for applications such as lightweight battery, super capacitor and anti-corrosion of metals.

1 INTRODUCTION

Electrically conjugated conducting polymers are considered to be the most promising conductive materials due to their unique electrical, magnetic and optical properties[1-5]. As a typical electrically conjugated conducting polymer, polythiophene (Pth) has been extensively investigated[6]. It may have widespread electrical applications such as supercapacitor, sensor, lightweight battery and anticorrosion of metals, due to its good thermal and oxidative stability, high charge carrier mobility and ease of fabrication[7-14].

In general, Pths are synthesized by the following five routes: i)

electro-polymerization[15-16], ii) chemical oxidative polymerization[17-18], iii) metal-catalyzed coupling reaction[19-20], iv) solid-state polymerization, [21] and v) acid catalyzed polymerization[22]. Among these methods, chemical oxidative polymerization has the advantages of wide monomer selection, easy of fabrication and high electric conductivity for the final product[23]. However, the rigid backbone and π-conjugation structure of Pth leads to poor solubility in common organic solvents and bad processability seriously, which limits its applications. One of the most effective ways to solve these problems is to directly synthesize polythiophene on a certain substrate. This method is the so-called one-step synthesis, avoiding the subsequent molding process[24-26]. Another approach is to use organic long-chain molecules as dopants and surfactants to provide Pth with good solubility and processability. Acetonitrile sodium dodecylsulfate, polyvinyl pyrrolidone and cetyltrimethylammonium bromide are used as dopants to synthesize Pth with different morghologies such as spherical and rod-like nanoparticles[27-29]. However, as far as we know, these reported Pths are water-insoluble.

This work reports for the first time on the synthesis of a novel liquid-like polythiophene. The structures of the as-synthesized L-Pth are characterized by Fourier transform infrared spectrometry (FTIR), ultraviolet-visible spectrophotometry (UV-vis), thermogravimetric analysis (TGA), and X-ray diffraction (XRD). The morphology of the L-Pth is assessed by transmission electron microscopy (TEM) and polarizing optical microscopy (POM). The rheological properties are evaluated by an ARES-RFS rheometer. The temperature dependency of the electric conductivity of the L-Pth is also studied. The fluorescence characteristics of L-Pth is tested by Fluorescence Spectrometer (FS), and it was used as a filler to prepare L-Pth/PVA composite films.

2 EXPERIMENTAL SECTION

2.1 Materials

Thiophene, dichloromethane, anhydrous ferric chloride, poly (vinyl alcohol) 1788 (PVA) and nonylphenol polyoxyethylene ether (NPES, $C_9H_{19}C_6H_4$-O-$(CH_2CH_2O)_{10}$-$CH_2CH_2CH_2SO_3H$) were purchased from Aladdin (Shanghai, China). All the reagents were used as received.

2.2 Preparation of L-Pth and L-Pth/PVA composite films

Synthesis of L-Pth: thiophene (0.02 mol) and NPES (0.01 mol) were dissolved in

a mixture of methylene chloride (80 mL) and water (5 mL) in a three-neck flask. The molar ratio between the monomer (thiophene) and dopant (NPES) was chosen as 2:1, which allows for the optimal doping of polythiophene [30-31]. $FeCl_3$ (0.05 mol) was then added to initiate the oxidative polymerization. The molar ratio of the monomer (thiophene) and initiator ($FeCl_3$) was chosen as 5:2 in order to control the polymerization rate of thiophene[32]. The mixture was stirred rigorously for 6 h at 3 °C. The resulting product was dialyzed with deionized water for 72 h using a cellulose dialysis membrane/bag (8000 g • mol^{-1} molecular weight cut off) to remove thiophene residual and oligomers. Finally, the purified L-Pth was dried under vacuum at 80 °C for 24 h. The neat polythiophene (Pth) was prepared with the same procedure but without NPES. Fig. 1 depicts the oxidative polymerization process of thiophene and L-Pth's structural formula [23].

Preparation of L-Pth/PVA composite films: the PVA was dispersed in water (10 wt.% of water). The L-Pth (0, 1 or 2 wt.% of PVA) was incorporated into PVA solution with stirring for 90 min. The water was evaporated by heating the mixture on a magnetic stir plate at 60 °C for 1h. Finally, L-Pth/PVA composite film was obtained after dried in a vacuum oven for 2 h to remove the water traces.

2.3 Characterization

Fourier transform infrared (FTIR) spectra of the Pth and L-Pth were recorded on a Nexus IR system (Thermo Nicolet Nexus, USA) using KBr pellets. The molecular weight distribution of the L-Pth was determined by gel permeation chromatography (GPC) (Ventura, CA, U.S.A.), equipped with a series of styragel columns. Water was used as an eluent at a flow rate of 1.5 μL • min^{-1}. Ultraviolet-visible (UV-vis) spectra were obtained by a Shimadzu UV-2550 spectrophotometer. A thermogravimetric analyzer (TGA, Netzsch STA 499C) was used to determine the loss in weight of the Pth and L-Pth under nitrogen at a heating rate of 10 °C • min^{-1} from 50 to 700 °C. Differential scanning calorimetry (DSC) was used to characterize endothermic and exothermic information from -70 to 20 °C at a rate of 10 °C • min^{-1}. A field-emission scanning electron microscope (FESEM, Hitachi S-4800) was used to analyze the Pth which was coated on the surface of copper foil. The morphology of the L-Pth at room temperature was characterized by a polarizing optical microscope (POM, Olympus BH-2) and a transmission electron microscope (TEM, Jeol JEM-2001F), respectively. XRD patterns were acquired on a D/Max-IIIA (Rigaku) diffractometer using Cu Ka radiation (Kα =1.54 Å). A fluorescence spectrometer (Hitachi, RF-5301PC) was used

to analyze the L-Pth dissolved in water. A digital multimeter (DT9203) was used to determine the temperature dependence of the electric conductivity in a homemade conductive mold.

3. RESULTS AND DISCUSSION

The chemical structures of the Pth, L-Pth and NPES were characterized using FT-IR spectroscopy. As shown in Fig. 2a, the Pth exhibits two absorption peaks at 1626 and 698 cm^{-1} corresponding to its stretching vibrations of C=C and C-S groups, respectively. The NPES shows an absorption peak at 1108 cm^{-1} corresponding to its $-SO_3^-$ group. As for the L-Pth, the absorption peak at 1661 cm^{-1} is assigned to stretching vibrations of the C=C group. Compared with the Pth's C=C group absorption peak, that of the L-Pth shows a significant shift from 1626 cm^{-1} f to 1661 cm^{-1}, implying that the NPES successfully dopes the L-Pth. To further ascertain the L-Pth's chemical structure, a UV-vis spectrum of L-Pth is analyzed, as shown in Fig. 2b. It offers an absorption peak at 276 nm corresponding to the π-π* transition of the phenyl moiety in NPES and the 2,5 substituted thiophene. A medium height around 428 nm and a very weak absorption peak around 620 nm belong to the π-π* transition of neutral thiophene moiety and HOMO-SOMO transition (or SOMO-LUMO transition) of radical cation thiophene moiety, respectively. Considering the observed polaron band is very weak, it is deduced that the proportion of the neutral thiophene moiety is larger than that of the p-doped polythiophene.

Table 1 shows the solubility of eigenstate Pth and L-Pth in various solvents. The Pth exhibits a low solubility except in DMF, a very powerful polar solvent, while the L-Pth is soluble in all the tested solvents (see Fig. 3). This can be attributed to the grafting of the NPES, whose flexible organic chain containing 10 oxyethylene groups helps to improve the solubility of the Pth in various solvents.

In order to detect the mass fraction of NPES in L-Pth, Pth in L-Pth was precipitated by an ammonia solution to remove the NPES. The mass percentage of NPES in the L-Pth could be calculated by the following equation:

$$f_{NPES} = (m_{L-Pth} - m_{Pth})/m_{L-Pth}$$

where m_{Pth} and $m_{L\text{-}Pth}$ are the mass of the Pth after dedoping and the L-Pth, respectively. Based on the experiment, the mass percentage of NPES in the L-Pth can be calculated: f_{NPES}= (1.05-0.16)/1.05=84.7%. According to the UV-vis analysis, a part of NPES molecules may be tightly bound by strong electrostatic interaction

between polythiophene bearing some positive charge and the sulfonate part of NPES, the rest of NPES molecules just surround polythiophenes by weak van der Waals interaction and π-π interaction between bound and unbound NPES molecules and between NPES and polythiophene molecules.

Fig. 4 shows the TGA curves of the Pth and L-Pth from 25 to 900 °C under nitrogen atmosphere. The loss in weight of the Pth proceeds in two stages: the first one is the decomposition of the polythiophene backbone from 270 to 410 °C; the other is that of the thiophene ring and its weight loss amounts to 55.9% when the temperature reaches 900 °C. For the L-Pth, three distinct regions of weightlessness are observed. The decomposition of the thiophene ring is involved in all regions. For NPES, the first stage of the weight loss appears from 170 to 270 °C and is associated with the decomposition of the $CH_2CH_2CH_2$ of the NPES. The second stage ranges from 270 to 410 °C and is attributed to the corruption of the carbon chain of polythiophene in the L-Pth and the $(CH_2CH_2O)_{10}$ in the NPES. It is noted that above 410 °C, polythiophene ring and benzene one continue to decompose. The amount of the final residue of the L-Pth is about 3.85%.

Fig. 5 shows the differential scanning calorimetry (DSC) curves of the Pth, NPES and L-Pth between -70 and 20 °C. The glass transition of the Pth does not appear in the above temperature range while that of NPES appears at -48 °C, and the L-Pth shows a glass transition at -60 °C. The fact that the glass transition of the NPES in the L-Pth is -60 °C while that of the NPES alone is -48 °C indicates higher flexibility of the L-Pth. The exothermic peak around -26.9 °C corresponds to the crystallization of the NPES. The endothermic peak around 0.9 °C is associated with the melting of the NPES. This melting temperature corroborates the liquid nature of the L-Pth at room temperature. The photograph inserted in Fig. 6b confirms that the L-Pth does flow under gravity at room temperature. The liquid properties of L-Pth are attributed to its special structure that a flexible organic shell covalent bonded onto a nanostructure surface. A similar hybrid nanostructure includes SiO_2[33], TiO_2[34], and carbon nanotubes[35].

Fig. 6 shows the storage modulus (G'), loss modulus (G″), and complex viscosity (η*) of the L-Pth as a function of temperature. As expected, they all gradually decrease with increasing temperature. The L-Pth exhibits a typical liquid behavior characterized by the fact that its G″ is always higher than G′ from 20 to 70 °C. Moreover, the viscosity is below 11 Pa·s over the whole test temperature range, further confirming the excellent

fluidity of the L-Pth. This suggests that the L-Pth has an excellent processability and can be readily mixed with many solvents.

Fig. 7a shows the SEM morphology of the Pth observed. It is a powder composed of particles from 1 to 50 μm in size. Figs. 7b and c show the morphologies of the liquid-like L-Pth observed under POM and TEM, respectively. It is composed of nanowires with 100−200 μm in length and 0.1-1 μm in diameter. Unlike the conventional polythiophene, the flexible chain on L-Pth improves the polythiophene segment'mobility, which makes the polythiophene main chain possess crystalline properties. The crystalline nature of the L-Pth is evidenced via its XRD pattern, as shown in Fig. 8a. The Pth is characterized by a broad diffraction peak from 15° to 30°, which could be ascribed to the scattering from its Pth chains's inter planar spacing. The crystalline nature of the L-Pth is confirmed by three sharp diffraction peaks at 14.8, 25.5 and 29.7°, respectively. The crystallinity (X_c) of the L-Pth can be written as:

$$X_c = \frac{Area\ of\ Crystalline\ Fraction}{Area\ of\ Crystalline\ Fraction\ +\ Area\ of\ Amorphus\ Fraction}$$

Fig. 8b shows the amorphous and crystal fitting curves of the L-Pth diffraction patterns, and the X_c of the L-Pth calculated from these curves is 7%.

Fig. 9 shows the temperature effect on the electric conductivity of the L-Pth. The latter increases from 0.1 to 1.2 S m^{-1} with increasing temperature from 25 to 65 °C. Typically, the variation tendency of the electric conductivity with temperature follows the VTF (Vogel-Tammann-Fulcher) equation[36]:

$$\sigma = A * \exp\left[-\frac{E_a}{R(T - T_0)}\right]$$

where σ is the electric conductivity, A is the prefactor related to the charge carrier concentration, E_a is the activation energy, R is the gas constant, T is the test temperature, T_0 is the Vogel temperature, typically taken as T_g-50 K. So, T_0 is 158 K based on the DSC result of the L-Pth.

Fig. 10a shows the excitation spectra of the L-Pth excited by lights of various wavelengths. The maximum excitation wavelength of the excitation spectrum is 515 nm. The intensity of the excitation wavelength increases first and then decreases with the increase of the emission spectrum wavelength. The optimal emission wavelength is 460 nm. Figs. 10b and c show the photographs of the L-Pth/PVA composite films under white light and blue light. The PVA reference film is colorless under white light and blue light (460 nm), while the L-Pth/PVA composite films become green under both white light and blue light. Short-wavelength radiation (rhodopsin spectrum) and the blue light hazard are shown to have significant impact on eye's health[37].

Considering the fluorescence characteristic of L-Pth that it turns high-energy blue light (in the ranges of 400 nm to 480 nm) into relative low-energy green light (peak at 515 nm), it could be used as a filler for anti-blue light eye protection film.

4 CONCLUSION

In summary, a novel liquid-like polythiophene is synthesized by chemical oxidative polymerization of thiophene. Unlike conventional polythiophene, L-Pth is composed of NPES and polythiophene, and part of NPES is doped on the thiophene backbone. It shows a liquid-like behavior and exhibits excellent electric conductivity. It turns high-energy blue light (460 nm) into relatively low-energy green light (peak 515 nm), showing that L-Pth/PVA composite films could have a potential for eye protection. Considering its superior solubility, processability and excellent electric conductivity, it may be a promising precursor for various applications such as the field of lightweight battery, supercapacitor and metal anticorrosion.

REFERENCES

[1] Aida, T.; E, W. Meijer.; S, I. Stupp. Functional Supramolecular Polymers. Science. 2012, 335, 813-817.

[2] Patterson, D.; Schnell, M.; Doyle, J. M. Enantiomer-pecific detection of chiral molecules via microwave spectroscopy. Nature. 2013, 497, 475–477.

[3] Yashima, E.; Ousaka, N.; Taura, D.; Shimomura, K.; Ikai, T.; Maeda, K. Supramolecular helical systems: helical assemblies of small molecules, foldamers, and polymers with chiral amplification and their functions. Chem. Rev. 2016, 116, 13752–13990.

[4] Taliani, C.; Danieli, R.; Zamboni, R.; Ostoja, P.; Porzio, W. Optical, electrical and structural comparative study of polycondensed thiophene based polymers. Synthetic Metals. 1987, 18(1-3), 177-182.

[5] Shi, Y.; Zhang, J; Bruck, A. M; Zhang, Y.; Li, J.; Stach, E. A. A tunable 3D nanostructured conductive gel framework electrode for high-performance lithium ion batteries. Advanced Materials. 2017, 29, 1603922.

[6] Louwet, F.; Groenendaal, L.; DHaen, J.; Manca, J.; Leenders, L.; Van Luppen, J.; Verdonck, E. PEDOT/PSS: synthesis, characterization, properties and applications. Synthetic Metals. 2003.

[7] Alvi, F.; Ram, M. K.; Basnayaka, P. A.; Stefanakos, E.; Goswami, Y.; Kumar, A. Graphene–polyethylenedioxythiophene conducting polymer nanocomposite based supercapacitor. Electrochimica Acta. 2011, 56(25), 9406-9412.

[8] Rosario-Canales, M. R.; Deria, P.; Therien, M. J.; Santiago-Avilés, J. J. Composite electronic materials based on poly(3,4-propylenedioxythiophene) and highly charged poly(aryleneethynylene)-wrapped carbon nanotubes for supercapacitors. ACS Applied Materials & Interfaces. 2012, 4(1), 102-109.

[9] de Leon, A. C. C.; Pernites, R. B.; Advincula, R. C. Superhydrophobic colloidally textured polythiophene film as superior anticorrosion coating. ACS applied materials & interfaces. 2012, 4(6), 3169-3176.

[10] Kousik, G.; Pitchumani, S.; Renganathan, N. G. Electrochemical characterization of polythiophene-coated steel. Progress in organic coatings. 2001, 43(4), 286-291.

[11] Wu, F.; Chen, J.; Chen, R.; Wu, S.; Li, L.; Chen, S.; Zhao, T. Sulfur/polythiophene with a core/shell structure: synthesis and electrochemical properties of the cathode for rechargeable lithium batteries. The Journal of Physical Chemistry C. 2011, 115(13), 6057-6063.

[12] Oh, S. H.; Lee, C. W.; Chun, D. H.; Jeon, J. D.; Shim, J.; Shin, K. H.; Yang, J. H. A metal-free and all-organic redox flow battery with polythiophene as the electroactive species. Journal of Materials Chemistry A. 2014, 2(47), 19994-19998.

[13] Wang, F.; Gu, H.; Swager, T. M. Carbon nanotube/polythiophene chemiresistive sensors for chemical warfare agents. Journal of the American Chemical Society. 2008, 130(16), 5392-5393.

[14] Li, B.; Santhanam, S.; Schultz, L.; Jeffries-El, M.; Iovu, M. C.; Sauvé, G.; Snyder, J. L. Inkjet printed chemical sensor array based on polythiophene conductive polymers. Sensors and Actuators B: Chemical. 2007, 123(2), 651-660.

[15] Hamnett, A.; Hillman, A. R. An ellipsometric study of the nucleation and growth of polythiophene films. Journal of the Electrochemical Society. 1988, 135(10), 2517-2524.
[16] Valle, M. A. D.; Gacitua, M.; Diaz, F. R.; Armijo, F.; Soto, J. P. Electro-synthesis and characterization of polythiophene nano-wires/platinum nano-particles composite electrodes. Study of formic acid electro-catalytic oxidation. Electrochimica Acta. 2012, 71, 277-282.
[17] Senthilkumar, B.; Thenamirtham, P.; Selvan, R. K. Structural and electrochemical properties of polythiophene. Applied Surface Science. 2011, 257(21), 9063-9067.
[18] Leclerc, M.; Faid, K. Electrical and optical properties of processable polythiophene derivatives: structure-property relationships. Advanced Materials. 1997, 9(14), 1087-1094.
[19] Arancon, D. R; SzeKiLin, C.; Vargas; Luque. To be or not to be metal-free: trends and advances in coupling chemistries. Organic & biomolecular chemistry. 2014, 12(1), 10-35.
[20] Babudri, F.; Farinola, G. M.; Naso, F. Synthesis of conjugated oligomers and polymers: the organometallic way. Journal of Materials Chemistry. 2004, 14.1, 11-34.
[21] Meng, H.; Perepichka, D. F.; Bendikov, M.; Wudl, F.; Pan, G. Z.; Yu, W.; Brown, S. Solid-state synthesis of a conducting polythiophene via an unprecedented heterocyclic coupling reaction. Journal of the American Chemical Society. 2003, 125.49, 15151-15162.
[22] Lowe, J.; Holdcroft, S. Poly (3-(2-acetoxyethyl) thiophene): a model polymer for acid-catalyzed lithography. Synthetic metals. 1997, 85, 1427-1430.
[23] Thanasamy, D.; Jesuraj, D.; Avadhanam, V. A novel route to synthesis polythiophene with great yield and high electrical conductivity without post doping process. Polymer. 2019, 175, 32-40.
[24] Lu, G.; Li, L.; Li, S.; Qu, Y.; Tang, H.; Yang, X. Constructing thin polythiophene film composed of aligned lamellae via controlled solvent vapor treatment. Langmuir. 2009, 25(6), 3763-3768.
[25] Samitsu, S.; Shimomura, T.; Heike, S.; Hashizume, T.; Ito, K. Field-effect carrier transport in poly(3-alkylthiophene) nanofiber networks and isolated nanofibers. Macromolecules. 2010, 43(19), 7891-7894.
[26] Lu, G.; Hong, W.; Tong, L.; Bai, H.; Wei, Y.; Shi, G. Drying enhanced adhesion of polythiophene nanotubule arrays on smooth surfaces. ACS Nano. 2008, 2(11), 2342-2348.
[27] Kadac, K.; Nowaczyk, J. Polythiophene nanoparticles in aqueous media. Journal of Applied Polymer Science. 2016, 133(23).
[28] Hofmann, A. I.; Kroon, R.; Yu, L.; Müller, C. Highly stable doping of a polar polythiophene through co-processing with sulfonic acids and bistriflimide. Journal of Materials Chemistry C. 2018, 6(26), 6905-6910.
[29] Wang, M., Huang, J.; Yang, Q.; Liu, Z.; Dong, L.; Wang, S.; Xiong, C. Synthesis and characterization of a fluid-like novel aniline pentamer. Macromolecular Research. 2018, 26(3), 233-237.

[30] Zotti, G. Doping-level dependence of conductivity in polypyrroles and polythiophenes. Synthetic metals. 1998,97(3), 267-272.
[31] Akimoto, M.; Furukawa, Y.; Takeuchi, H.; Harada, I.; Soma, Y.; Soma, M. Correlation between vibrational spectra and electrical conductivity of polythiophene. Synthetic metals. 1986,15(4), 353-360.
[32] Olinga, T.; François, B. Kinetics of polymerization of thiophene by $FeCl_3$ in choloroform and acetonitrile. Synthetic Metals. 1995, 69(1-3), 297-298.
[33] Bourlinos, A. B.; Herrera, R.; Chalkias, N; Jiang, D. D; Zhang, Q.; Archer, L. A. Surface-functionalized nanoparticles with liquid-like behavior. Advanced Materials, 2005,17(2), 234-237.
[34] Bourlinos, A. B.; Chowdhury, S. R.; Herrera, R.; Jiang, D. D.; Zhang, Q; Archer, L. A. Functionalized nanostructures with liquid-like behavior: expanding the gallery of available nanostructures. Advanced Functional Materials, 2005,15(8), 1285-1290.
[35] Bourlinos, A. B.; Georgakilas, V.; Tzitzios, V.; Boukos, N.; Herrera, R. Giannelis, E. P. Functionalized carbon nanotubes: synthesis of meltable and amphiphilic derivatives. Small,2006, 2(10), 1188-1191.
[36] Diederichsen, K. M.; Buss, H. G.; McCloskey, B. D. The compensation effect in the Vogel–Tammann–Fulcher (VTF) equation for polymer-based electrolytes. Macromolecules. 2017, 50(10), 3831-3840.
[37] Algvere, P. V.; Marshall, J.; Seregard, S. Age-related maculopathy and the impact of blue light hazard. Acta Ophthalmologica Scandinavica. 2006, 84(1), 4-15.

Table 1 Solubility of the Pth and L-Pth in various solvents

Solvent	Pth	L-Pth
Water	Insoluble	soluble
Ethanol	Insoluble	soluble
Methylene Chloride (MC)	Insoluble	soluble
Dimethyl formamide (DMF)	Slightly soluble	soluble
Dimethyl sulfoxide (DMSO)	Insoluble	soluble
Tetrahydrofuran (THF)	Insoluble	soluble

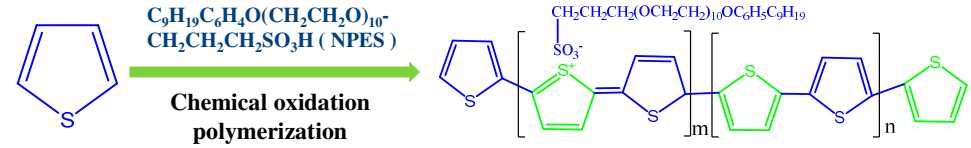

Thiophene **L-Pth**

Fig. 1 Scheme of the preparation process of the L-Pth.

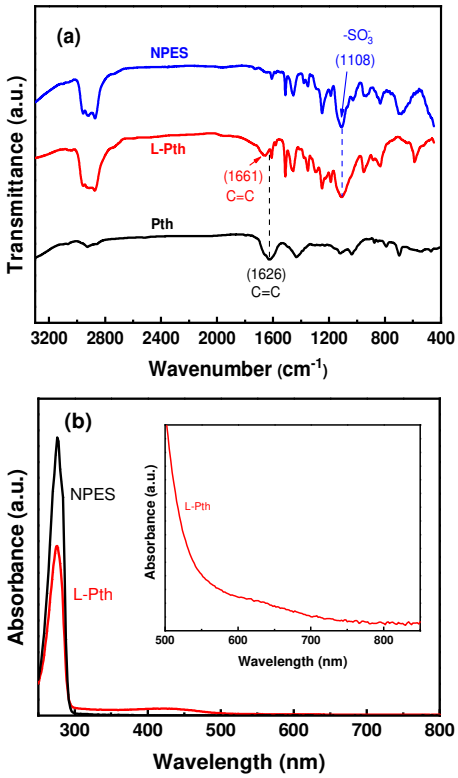

Fig. 2(a) FT-IR spectra of the Pth, NPES and L-Pth; (b) UV-vis spectrum of the L-Pth.

Fig. 3 Photographs of the L-Pth’s dissolution in various solvents.

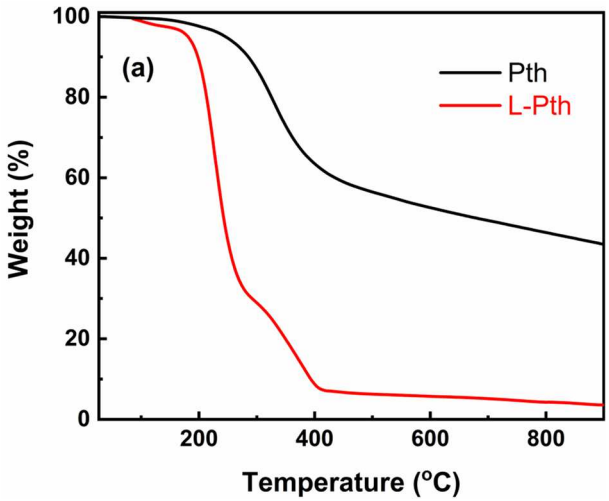

Fig. 4 Thermogravimetric analysis (TGA) curves of the Pth and L-Pth. Heating rate: 10 °C • min^{-1}

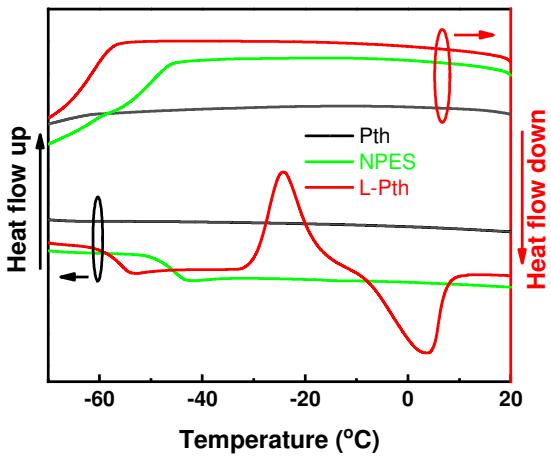

Fig. 5 Differential scanning calorimetry (DSC) curves of Pth, NPES and L-Pth.

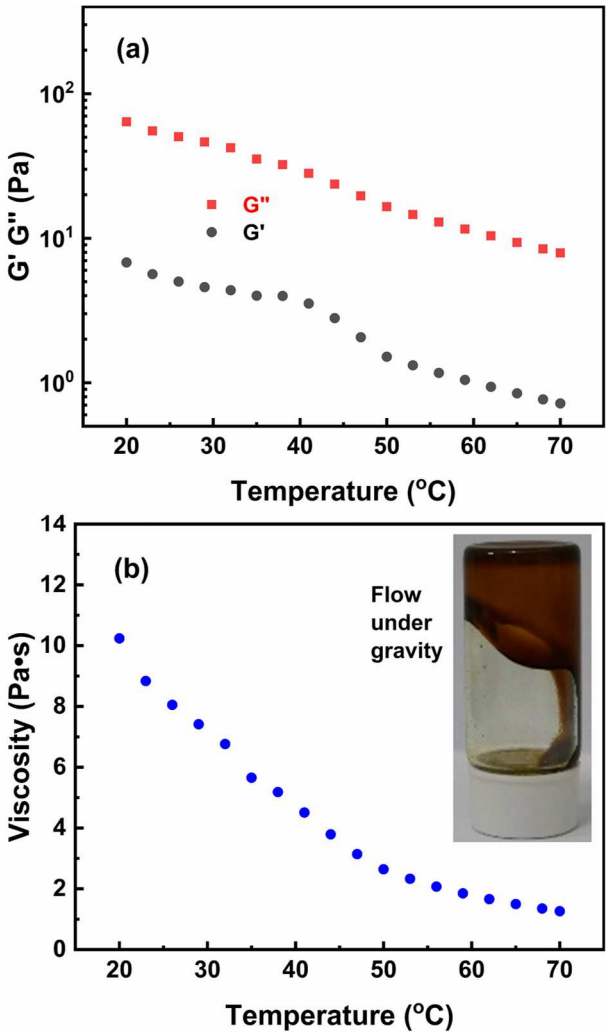

Fig. 6 Temperature-dependent storage (G') and loss (G") moduli (a) and viscosity (b) of the L-Pth.

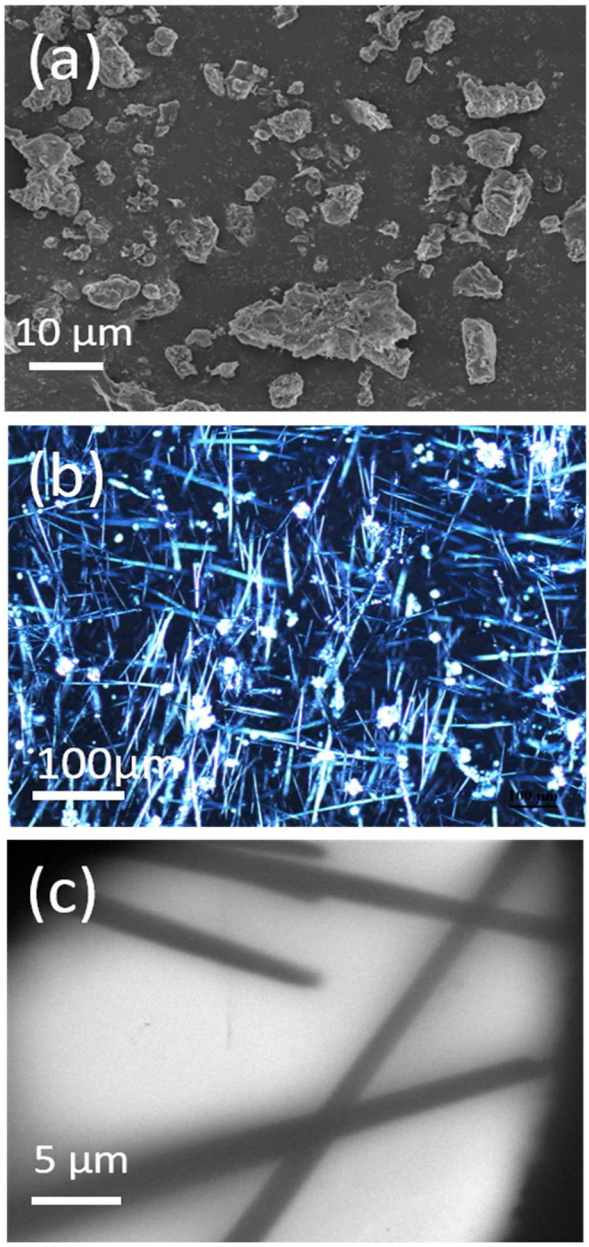

Fig. 7 (a) SEM of Pth; (b) POM of L-Pth; (c) TEM of L-Pth.

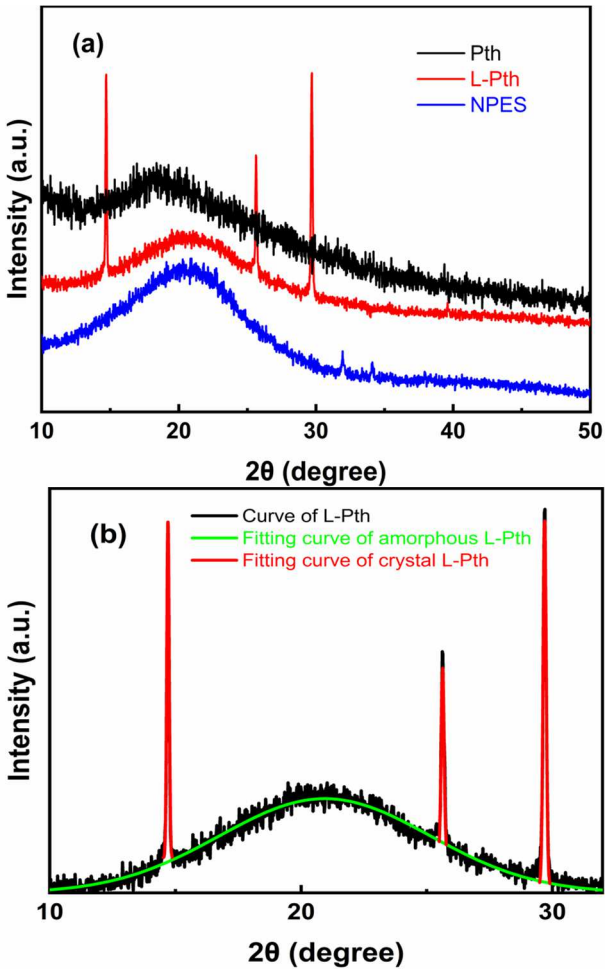

Fig. 8 (a) XRD patterns of Pth, NPES and L-Pth; (b) amorphous and crystal fitting curves of L-Pth diffraction pattern.

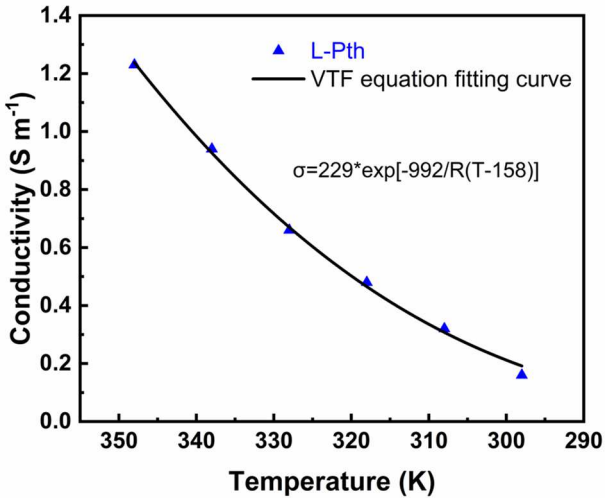

Fig. 9 Conductivity of the L-Pth as a function of temperature and VTF equation fitting curve.

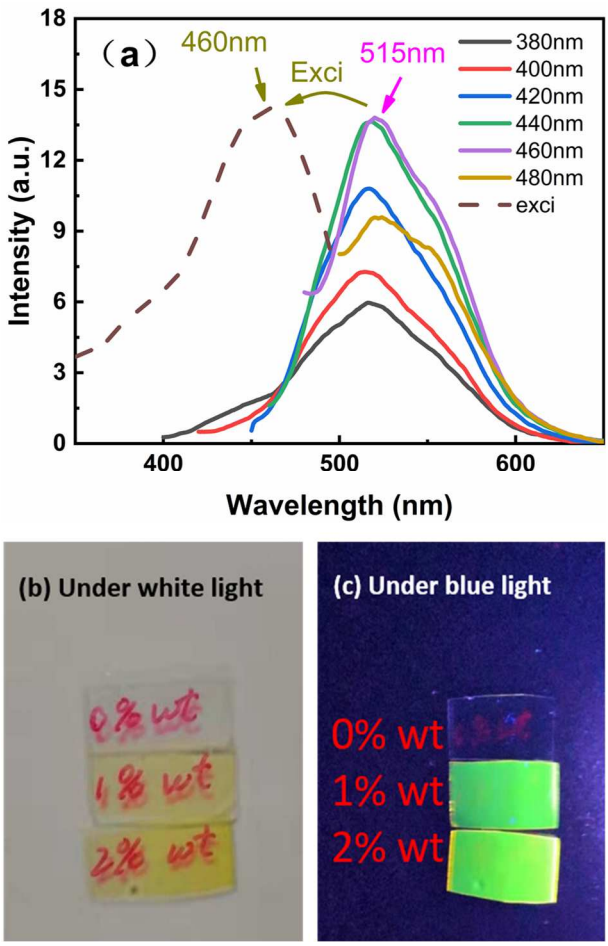

Fig. 10 (a) Excitation spectra of the L-Pth excitated by lights of various emission lights; (b, c) Photographs showing L-Pth/PVA composite films under white light and blue light (460 nm).